CHEMISTRY OF MATERIALS

pubs.acs.org/cm

Article

Harvest the Polyanion Rotation in Sodium Superionic Conductors?

Yu Yang, Chaohong Guan, Runxin Ouyang, and Hong Zhu*

Cite This: *Chem. Mater.* 2024, 36, 3776−3785

Read Online

ACCESS | Metrics & More | Article Recommendations | Supporting Information

ABSTRACT: The existing design principles and screening strategies of superionic conductors predominantly focus on the perspective of a static crystal structure. However, the dynamic mechanism involving anion rotational motion as well as its interaction with cation translational motion has received less exploration, especially in the realm of the accelerated discovery of new fast ionic conductors with these strong dynamic couplings. Herein, we design a multistep density functional theory molecular dynamics (DFT-MD) high-throughput workflow based on the structural feature of an isolated framework to rapidly screen Na superionic conductors with polyanion rotation. Interpretable machine-learning classification indicates that structures with larger atomic volumes and smaller polyanions tend to exhibit anion rotational behavior. Building on the observation of persistent, large-angle anion reorientation and the time-spatial correlation of Na hops and polyanion rotations, we identified polyanion rotation behavior for the first time in 10 new compounds and quantified the contribution of polyanion rotation to Na diffusion, among which three are novel Na superionic conductors with significant cation−anion dynamics coupling, including $NaGaBr_4$, $NaNbCl_6$, and Na_4SiSe_4. Additionally, we developed highly accurate moment tensor potentials for $NaNbCl_6$ and Na_4SiSe_4. Long time scale machine-learning molecular dynamics simulations (MLMD) at 300 K revealed that the anion rotation still exists in $NaNbCl_6$ at room temperature, while Na_4SiSe_4 displays non-Arrhenius behavior. This study provides valuable guidance for the development of new fast ion conductors utilizing polyanion rotation.

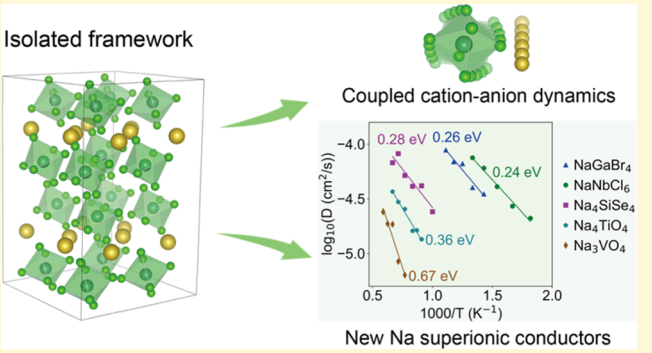

INTRODUCTION

As the need for electricity continues to grow and current energy sources rely heavily on limited fossil fuels, the development of advanced battery materials has become a crucial factor in both electrifying transportation and storing renewable energy.[1−3] All-solid-state batteries (ASSBs), in which solid electrolytes (SEs) are used as substitutes for flammable organic liquid electrolytes (LEs), provide not only higher safety but also potentially enable the applications of high-voltage cathodes and metal anodes to realize higher energy densities.[4] Furthermore, solid-state sodium-ion batteries are considered a more cost-effective alternative to their lithium-ion counterparts due to the abundance of sodium in the Earth's crust.[5−7] A key criterion for making ASSBs a reality is the development of SEs with sufficient ionic conductivity (>1 mS/cm at room temperature).[8]

To accelerate the discovery of novel superionic conductors, some structural features related to the fast transport of alkali metal ions have been proposed. Specifically, Ceder et al. found that the body-centered-cubic arrangement of anion framework is preferred over close-packed structures.[9] This feature has been observed in high-performing sulfide ionic conductors, such as $Li_{10}GeP_2S_{12}$ and $Li_7P_3S_{11}$. Subsequently, they demonstrated that the corner-sharing connectivity of oxide crystal structure framework boosts superionic conductivity.[10] These readily accessible structural properties have successfully guided the high-throughput screening of new superionic conductors.[10−12] However, the current design principles of SEs are mainly proposed from the perspective of static structure, the lattice dynamics for Li diffusion and polyhedron rotation in SEs has been relatively less explored.[13,14] By utilizing neutron powder diffraction and ab initio molecular dynamics simulations (AIMD), anion rotation behavior has been captured in a few SEs, including $Na_{11}Sn_2PX_{12}$ (X = S, Se),[15] Li_3PS_4,[16,17] $Na_{2.25}Y_{0.25}Z_{0.75}Cl_6$,[4] argyrodite,[18,19] and antiperovskite,[20,21] for which anion rotation motion is reported to facilitate cation translational motion, so-called the paddle-wheel effect (as illustrated in Figure 1a). It should be stressed that anion rotation does not necessarily contribute to cation diffusion. For instance, Sun et al. proven that the enhanced conductivity in BH^{4-} substituted Li argyrodite mainly derives from the weak interaction between Li and BH^{4-} polyanions instead of the usually expected paddle-wheel effect arising from

Received: January 13, 2024
Revised: March 28, 2024
Accepted: March 28, 2024
Published: April 10, 2024

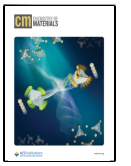

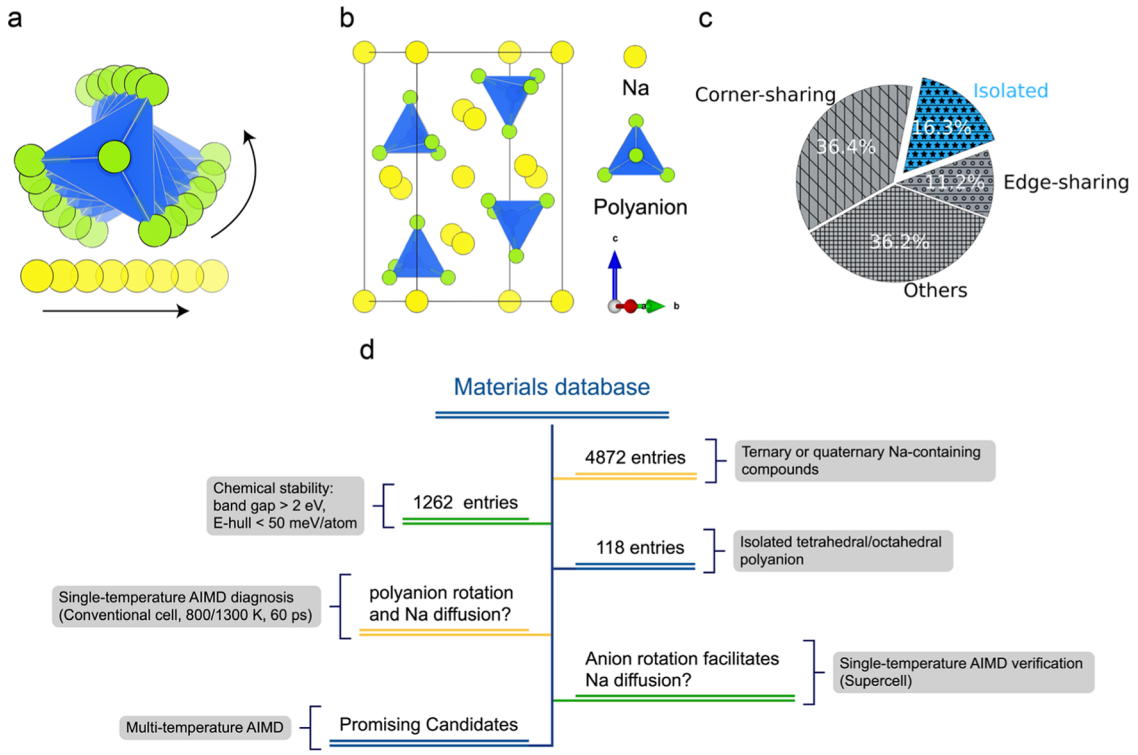

Figure 1. Screening for new superionic conductors with coupled cation−anion dynamics based on an isolated framework. (a) Schematic diagram of the paddle-wheel effect. (b) The structure with isolated framework is illustrated. (c) Pie chart of framework connectivity types for Na-containing ternary and quaternary compounds from the Materials Project (MP) database, with a total of 4872 compounds. (d) Flowchart of the multistep high-throughput screening.

anion rotation.[18] Xu et al. found that the rotation of PS_4^{3-} polyanion is only slightly correlated with Li diffusion in $Li_7P_3S_{11}$ at room temperature, and even has weakly negative impacts on the overall Li ion diffusion.[22]

Therefore, it is indispensable to conduct a comprehensive and detailed investigation into the rotational dynamics as well as its coupling with cation diffusion, from which the mechanism and descriptors for anion rotation as well as its coupling with cation transport could be extracted and applied to the SE design. Additionally, the high cost of AIMD simulations means that they are typically performed at elevated temperatures to obtain sufficient diffusion statistics, and the AIMD simulation temperatures for reported SEs with anion rotation are all above 600 K.[4,15,16,18,20,23] Whether anion rotation can be sustained at room temperature (300 K), which is more relevant to the application of solid-state batteries, requires further exploration. The recently emerging molecular dynamics simulation based on the machine-learning interatomic potentials[22,24−26] (MLMD) make it possible to study the anion rotation behavior of SEs at low temperature and long time scale with near density functional theory (DFT) accuracy in energies and forces.

In this work, we design a multistep high-throughput workflow based on the structural feature of isolated framework to screen novel Na superionic conductors with polyanion rotation dynamics. Interpretable machine-learning (ML) classification reveals that the structures with a large volume per atom (VPA) and small polyanion are more likely to exhibit anion rotational behavior. For the first time, we captured the phenomenon of polyanion rotation in $NaXY_4$ (X = In, Al, Ga; Y = I, Br), $NaXCl_6$ (X = Ta, Nb), Na_4SiSe_4, Na_4TiO_4, Na_3XO_4 (X = V, As), and Na_3NO_4. We identify three novel Na superionic conductors: $NaGaBr_4$, $NaNbCl_6$, and Na_4SiSe_4 with pronounced cation−anion dynamics coupling through a comprehensive analysis and quantification of the correlation between polyanion rotational motion and Na translational motion from AIMD simulations. Moreover, we developed machine-learning interatomic potentials with high accuracy for $NaNbCl_6$ and Na_4SiSe_4 and performed long time scale (100 ns) MLMD simulations at 300 K. The results show that the anion rotation is still present in $NaNbCl_6$ at room temperature, while Na_4SiSe_4 exhibits non-Arrhenius behavior. Furthermore, $Na_{3.75}SiSe_4$ exhibits an enhanced Na diffusion and a more intense reorientation of $SiSe_4$ at 300 K compared to Na_4SiSe_4. We suggest that for potential superionic conductors that exhibit the coupled cation−anion dynamics at elevated temperatures, the introduction of Na vacancies can effectively promote both polyanion rotation and Na diffusion toward low-temperature ranges.

RESULTS AND DISCUSSION

Screening and Classification of Polyanion Rotation Behavior. As mentioned in the Introduction section, the reported SEs with anion rotation[4,15−21] have a common structure feature, namely, an isolated framework, where the non-Li/Na cation polyhedrons (polyanions/cluster-ions) in these structures are disconnected, and never share any common corners, edges, or faces, as shown in Figure 1b. This isolated framework not only provides degrees of freedom for anion rotation but also possesses a three-dimensional (3D) Na-ion diffusion pathway; thus, it can be used as a structure descriptor to screen potential superionic conductors with polyanion rotation. By identifying the connectivity of framework for ternary and quaternary Na-containing compounds in

https://doi.org/10.1021/acs.chemmater.4c00102
Chem. Mater. 2024, 36, 3776−3785

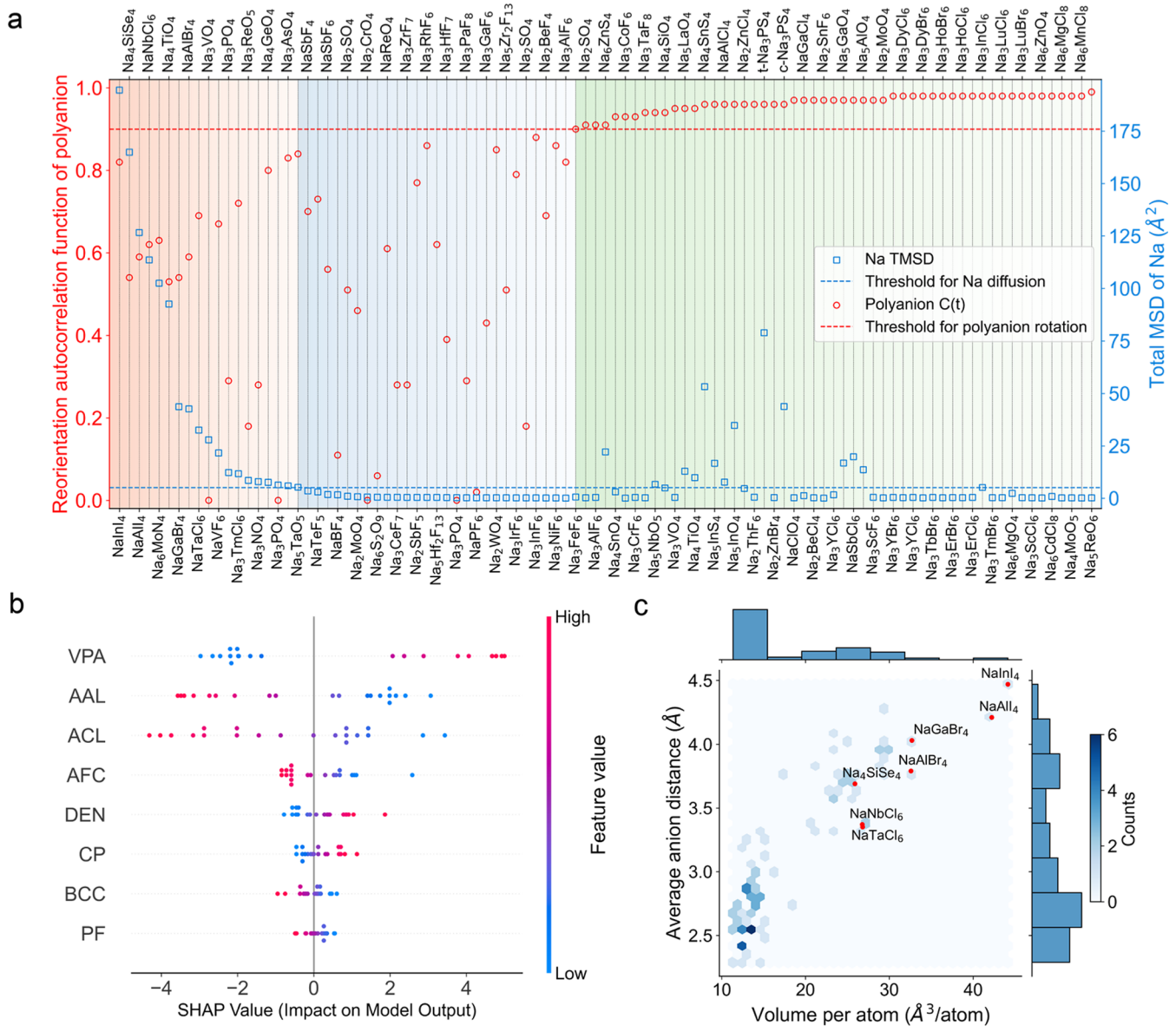

Figure 2. Classification of compounds with or without polyanion rotation. (a) $C(t)$ of polyanion (red circles, left axis) and TMSD of Na (blue squares, right axis) for 99 stable isolated frameworks at the single-temperature AIMD diagnosis step. Different background shades represent different categories classified based on threshold (red and blue dotted line). (b) Shapley Additive exPlanations (SHAP) feature importance for an optimal logistic regression model with 8 features, the red and blue colors indicate high and low values of a given feature, respectively. (c) Hexbin plot of volume per atom (VPA) versus average anion distance (AAL) for 99 isolated frameworks, with some compounds in category 1 marked with red dots.

the Materials Project (MP) database,[27] the percentage of framework types for isolated, corner-sharing, edge-sharing, and others (mixed type) are 16.3, 35.4, 11.2, and 36.2%, respectively, as depicted in Figure 1c. The abundance of the isolated framework offers fertile ground to dig for high-throughput searching.

Figure 1d displays a multistep high-throughput workflow starting from 4872 ternary and quaternary Na-containing compounds in the MP database. Considering the electrochemical and phase stability for SEs, 1262 compounds with a band gap more than 2 eV and the energy above the hull (E_{hull}) below 50 meV/atom are retained. Next, a total of 118 compounds with isolated tetrahedral or octahedral polyanions are obtained by identifying framework connectivity. Due to the high computational cost of AIMD simulation on supercell size, we first perform a single-temperature AIMD diagnosis of 60 ps on conventional cell for 118 isolated frameworks to observe whether the polyanion rotation and Na diffusion occur; this method has been used in previous work.[28] The AIMD simulation temperature is set to 800 K for compounds with a monovalent anion framework (F/Cl/Br/I) and to 1300 K for those with a divalent anion framework (O/S/Se), in reference to the parameter settings for halide,[29] sulfide,[30] and oxide.[31] Then, for these compounds with both polyanion rotation and Na diffusion, well converged single-temperature AIMD simulations are performed on a supercell with at least 8 Å along each lattice direction to verify and analyze the dynamic correlation between anion rotational motion and Na translational motion. Finally, multitemperature AIMD simulations are performed to estimate activation energy and room-temperature

https://doi.org/10.1021/acs.chemmater.4c00102
Chem. Mater. 2024, 36, 3776−3785

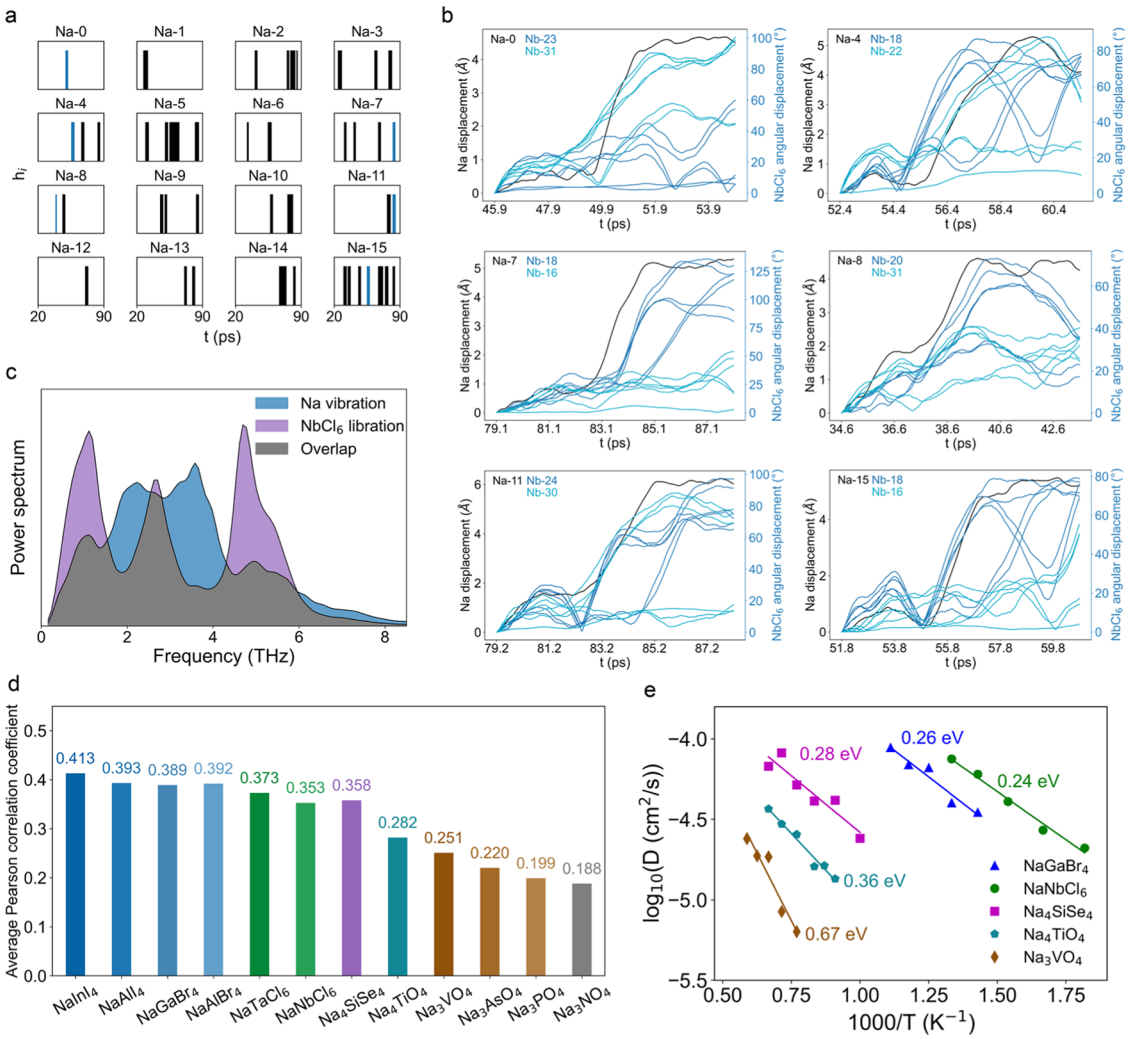

Figure 3. Correlation between Na diffusion and polyanion rotation for potential superionic conductors. (a) Identification of long-lived Na migration events for $NaNbCl_6$ at 600 K AIMD simulation. Each rectangle individually plots h_i vs simulation time for the 16 Na ions in supercell, and each vertical line ($h_i = 1$) in the rectangle represents a long-lived Na migration event of at least a distance a (a = 3.8 Å) occurring at simulation time t. (b) Each plot shows the translational displacements of Na (black line, left axis) and angular displacements of the two nearest-neighbor $NbCl_6$ polyanions (blue hues, right axis), corresponding to six migration events marked with blue vertical lines in panel (a), respectively. The ID for Na and $NbCl_6$ is marked in the top left corner of each plot. Six angular displacements are plotted for each $NbCl_6$ polyanion using the same color, corresponding to the rotational motion of Six Cl atoms around the center of mass of the $NbCl_6$ polyanion. (c) Power spectrum calculated via the Fourier transform of linear velocity autocorrelation of Na and angular velocity autocorrelation of $NbCl_6$ for $NaNbCl_6$ at 300 K AIMD simulation. (d) For 12 candidates, the average Pearson correlation coefficient between the angular displacement of C−Na and C−A bond (C denotes the central atom of the polyanion, and A denotes the anion closest to Na) for all events in which Na stays within the first shell of polyanion during whole simulation time, identical structure groups were shown in the same hues. (e) Arrhenius plots of Na-ion diffusivity in $NaGaBr_4$, $NaNbCl_6$, Na_4SiSe_4, Na_4TiO_4, and Na_3VO_4 from AIMD simulations.

Na-ion conductivity for these compounds with coupled cation−anion dynamics. The detailed discussion is presented below.

At the single-temperature AIMD diagnosis step, we first excluded 19 structures with melting frameworks whose non-Na cation total mean square displacement (TMSD) exceeds 2 $Å^2$. Then, the reorientation autocorrelation function $C(t)$ of the polyanion (see the Methods section for details) and the Na TMSD for 99 stable isolated frameworks are calculated, as shown in Figure 2a. The $C(t)$ threshold for detecting polyanion rotation is set to 0.9 (red dash line in Figure 2a); it is considered that the anion undergo significant reorientation if $C(t)$ is below this value.[32] Similarly, the TMSD threshold for determining Na diffusion is set to 5 $Å^2$ (blue dashed line), implying that the average hopping distance of Na is at least 2.2 Å. In this context, the compounds with both polyanion rotation and Na diffusion (19 entries), with polyanion rotation but no Na diffusion (27 entries), and without polyanion rotation (53 entries) are classified as category 1 (red shading in Figure 2a), category 2 (blue shading), and category 3 (green shading), respectively. Detailed data are provided in Supporting Information, Table S1.

To gain more insight into the factors affecting polyanion rotation, machine learning (ML) is used to classify the 99 isolated frameworks as rotation (46 entries including category 1 and category 2) or nonrotation (53 entries of category 3). Supporting Information, Table S2 lists 23 features that potentially influence polyanion rotation. The selection of features is based on physical intuition and previous literature reports.[6,33,34] These features are categorized into four groups

https://doi.org/10.1021/acs.chemmater.4c00102
Chem. Mater. 2024, 36, 3776−3785

based on their nature: "structural", "local geometrical", "electrostatic", and "elemental". The Pearson correlation map between the candidate features is depicted in Supporting Information, Figure S1. The redundant features with a correlation higher than 0.9 with other features were eliminated, leaving 19 features (Supporting Information, Table S2). Then, four ML algorithms[35] are employed to evaluate the binary classification models in a 10-fold cross-validation loop, where each iteration has a 72/18/10 train/validation/test split and hyperparameters are optimized on the validation set. The results of the 10-fold cross-validation and hyperparameters are shown in Supporting Information, Tables S3 and S4. The logistic regression model outperforms other tree-based models (Random Forest, XGBoost, and LightGBM) with the F1 score of 0.73. To avoid overfitting the small data set including 99 samples with 19 features, we built logistic regression models using all possible subsets of the 19 nonredundant features to determine the optimal combination and number of features. Supporting Information, Figure S2 shows that the F1 score initially increases with the number of features and then decreases, reaching a maximum value (F1 score = 0.85) at an 8-feature model. To interpret the contribution of each feature to the model output, Shapley Additive exPlanations[36] (SHAP) is used to analyze the optimal 8-feature logistic regression model results, as shown in Figure 2b. The top two most important features related to the rotation of polyanions are the volume per atom (VPA) and average anion distance (AAL). Increasing the VPA, which means a larger free volume within the structure, leads to a greater predicted probability of rotation. Additionally, increasing the AAL leads to decreased probability for rotation, indicating that smaller polyanions are advantageous for rotation. Figure 2c shows a hexbin plot of the two variables, VPA and AAL, for 99 isolated frameworks. As expected, some compounds in category 1 (marked with red dots) typically have a larger VPA. Of course, the factors affecting anion rotation are diverse, but these simple descriptors, such as VPA and AAL, can help us quickly screen for compounds with anion rotation.

Novel Superionic Conductors Featuring Coupled Cation−Anion Dynamics. To precisely analyze the dynamic relationship between anion rotation and Na diffusion, well converged AIMD simulations were performed on supercell for all compounds in category 1 (the statistical variance of the diffusion coefficient is shown in Supporting Information, Figure S3). Viewed from species projection MSD (Supporting Information, Figure S4) and $C(t)$ of polyanion (Supporting Information, Figure S5), we identified 12 candidates that still exhibited significant Na diffusion and polyanion rotation, including $NaInI_4$, $NaAlI_4$, $NaGaBr_4$, $NaAlBr_4$, $NaTaCl_6$, $NaNbCl_6$, Na_4SiSe_4, Na_4TiO_4, Na_3VO_4, Na_3AsO_4, Na_3PO_4, and Na_3NO_4. These 12 candidates were classified into 6 distinct structure groups using a structural matching algorithm[37] (anonymizing the species of the nonsodium cation and anion), namely, $NaXY_4$ (X = In, Al, Ga; Y = I, Br), $NaXCl_6$ (X = Ta, Nb), Na_4SiSe_4, Na_4TiO_4, Na_3XO_4 (X = V, As, P), Na_3NO_4, respectively. It is noteworthy that although the polyanions of Na_3XO_4 (X = V, As, P) show the fastest rotation, their Na TMSD is relatively low, implying the weak correlation between Na and anion dynamics in this structure group. For these candidates, polyanion rotational disorder is also verified by the anion probability density function (Supporting Information, Figure S6), where the anion randomly appears around the non-Na cation and forms a cage-like iso-surface. In addition, the bond length of the cation and its anion ligands in polyanion display only slight fluctuations due to atomic vibration or rotation during the whole AIMD simulations, indicating that the frameworks are stable even at elevated temperature, as demonstrated in Supporting Information, Figure S7. To the best of our knowledge, this is the first observed instance of polyanion rotation in these compounds except for Na_3PO_4[38] and our previously reported Na_4SiSe_4.[39]

As we mentioned before, significant polyanion rotation does not necessarily lead to fast Na diffusion. To determine the correlation between anion rotational motion and Na translational motion, we thoroughly analyzed the AIMD trajectories of 12 candidates with both polyanion rotation and Na diffusion. Taking $NaNbCl_6$ as an example, all long-lived Na migration events were first identified using the functional $h_i(t, a, \Delta t, t_a)$ (see the Methods section for details), as shown in Figure 3a. Each rectangle individually plots h_i vs simulation time for the 16 Na ions in simulation supercell, and each vertical line ($h_i = 1$) in rectangle represents a long-lived Na migration event with a minimum distance a (a = 3.8 Å) occurring at simulation time t. We then selected six representative Na migration events (blue vertical line in Figure 3a), tracking the translational displacement of Na and the angular displacement of the two nearest-neighbor $NbCl_6$ polyanions, as shown in Figure 3b. A clear pattern was observed for these migration events, where significant Na displacement (at least 3.8 Å) and sustained $NbCl_6$ angular displacement (60−140°) occur almost simultaneously. Displacement plots for more migration events are shown in Supporting Information, Figure S8; these data also demonstrate that the displacements of Na and $NbCl_6$ occur at the same time window and have a common shape. This strong temporal and spatial correlation between the translational motion of Na and the rotational motion of $NbCl_6$ suggests the existence of coupled cation−anion dynamics in $NaNbCl_6$. The power spectrum for Na vibration and $NbCl_6$ libration via the Fourier transform of the linear velocity autocorrelation function of Na and the angular velocity autocorrelation function of $NbCl_6$ was calculated to further corroborate the origin of dynamics correlation, as shown in Figure 3c. The vibration spectrum of Na shows a broad dispersion in the range of 0−7 THz; these Na low-frequency modes are characteristic of large vibrational amplitudes.[40] The libration spectrum of $NbCl_6$ has a peak near 1, 2.5, and 5 THz, corresponding to the $NbCl_6$ rotational modes. There is a large overlap between the Na and the $NbCl_6$ spectrum in the low-frequency region, indicating that there are coupled dynamics between Na vibration and $NbCl_6$ libration.

For other candidates, analogous analyses were also performed to investigate the correlation between anion rotational motion and Na translational motion, and the results are shown in Supporting Information, Figures S9−S19. In $NaInI_4$, $NaAlI_4$, $NaGaBr_4$, $NaAlBr_4$, $NaTaCl_6$, and Na_4SiSe_4, a pattern similar to that of $NaNbCl_6$ was observed. Specifically, in the majority of migration events, both Na displacement and polyanion angular displacement happen almost simultaneously. Additionally, both the power spectra of Na vibration and polyanion libration are entirely distributed in the low-frequency (<8 THz) region. These soft phonon modes of Na and anion may lead to shallower potential energy surfaces that favor Na diffusion. On the other hand, for Na_4TiO_4, Na_3VO_4, Na_3AsO_4, Na_3PO_4, and Na_3NO_4, more migration events exhibit asynchrony, where the angular displacement of

https://doi.org/10.1021/acs.chemmater.4c00102
Chem. Mater. 2024, 36, 3776−3785

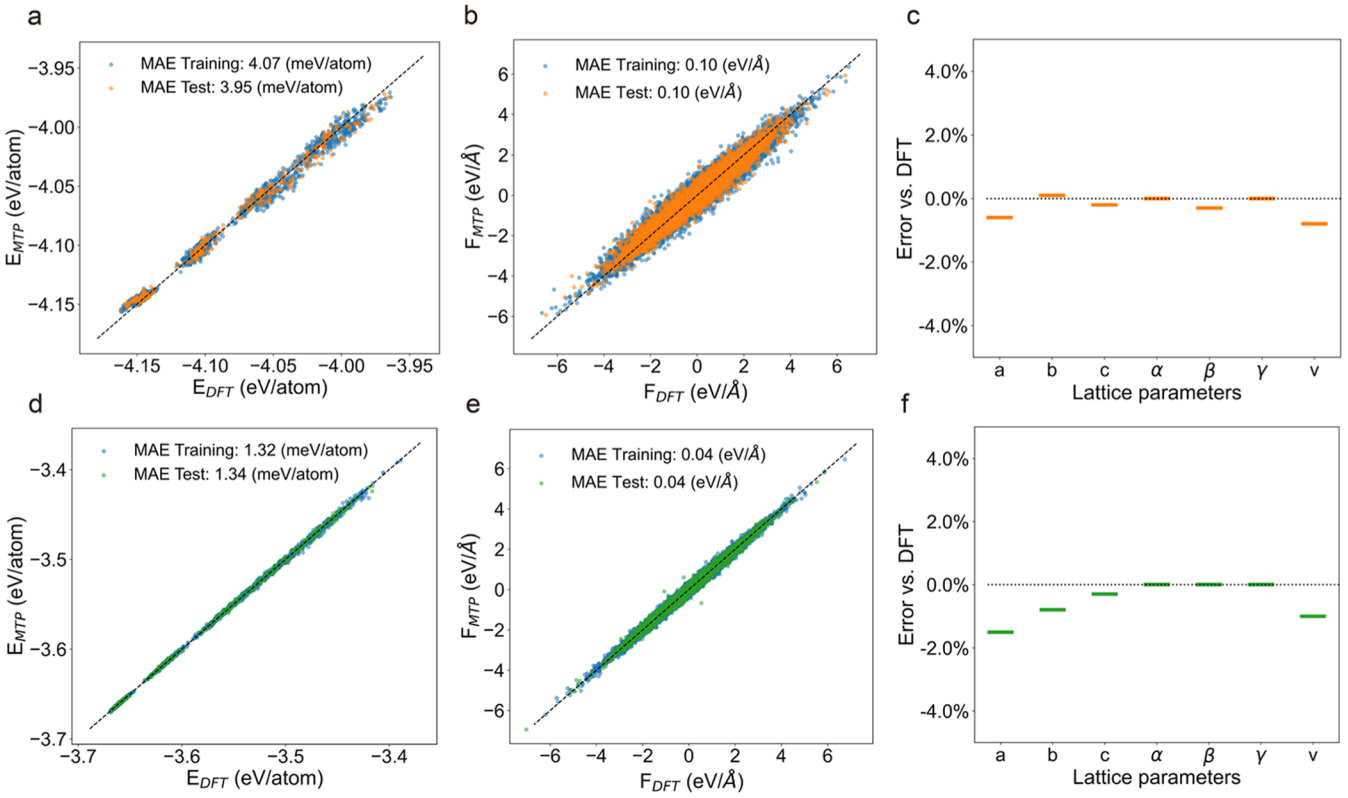

Figure 4. Plots of the MTP predicted versus DFT energies, forces, and lattice parameters for $NaNbCl_6$ (a–c) and Na_4SiSe_4 (d–f).

the polyanions either precedes or follows Na displacement, with a temporal gap of 2–4 ps. Meanwhile, the power spectra of polyanion libration show a higher density in midfrequency region (10–15 THz) contrast to that of Na vibration (0–10 THz) for these candidates, meaning that the majority of polyanion libration does not occur on the same time scale as Na vibration.

To quantitatively determine the difference in the correlations between anion rotational motion and Na translational motion for 12 candidates, we tracked all of the "events" for which Na stays within the first shell of polyanion during the whole simulation time. For each of the events, we obtained a time series of angular displacement for C–Na and C–A bonds (C denotes the central atom of the polyanion, and A denotes the anion closest to Na). Then, the Pearson correlation coefficient of these two angular displacements was calculated. Supporting Information, Figure S20 shows the probability distribution of the Pearson correlation coefficient. In agreement with the preceding analysis, there is a broader distribution in regions with a Pearson correlation coefficient larger than 0.5 for $NaInI_4$, $NaAlI_4$, $NaGaBr_4$, $NaAlBr_4$, $NaTaCl_6$, $NaNbCl_6$, and Na_4SiSe_4, suggesting a stronger correlation between anion rotation and Na diffusion in these candidates. Most coefficients for Na_4TiO_4, Na_3VO_4, Na_3AsO_4, Na_3PO_4, and Na_3NO_4 are less than 0.5. Since correlations below 0.5 are generally considered statistically weak, it suggests a lack of significant correlation between Na displacement and anion group rotation in these materials. The average Pearson correlation coefficients for 12 candidates are shown in Figure 3d, and this value can be used as a metric to measure the degree of coupling between the anion rotational motion and Na translational motion. The Arrhenius plots (Figure 3e) show that the fitted activation energies of $NaNbCl_6$, $NaGaBr_4$, and Na_4SiSe_4 are 0.24, 0.26, and 0.28 eV, respectively, and the corresponding extrapolated room-temperature Na ionic conductivities are 7.67, 3.06, and 1.42 mS/cm. The excellent conductivity of these compounds can be ascribed to significant cation–anion dynamics coupling (higher value of average Pearson correlation coefficients, Figure 3d). Contrarily, Na_4TiO_4 (E_a = 0.36 eV, $\sigma_{300\,K}$ = 0.09 mS/cm) and Na_3VO_4 (E_a = 0.67 eV) exhibit higher activation energies and seem not to benefit from free anion rotations obviously. To further investigate the interdependence of the Na diffusion and anion rotation, we performed AIMD simulations on 12 candidates by freezing one type of ion to observe the effect of this constraint on the mobility of the other type of ion. As shown in Supporting Information, Figure S21, we found that for all materials, freezing the anions completely quenches the diffusion of Na, and freezing the Na ions also completely restricts the rotation of anions. These results imply that in our candidate materials, the rotation of anions is a necessary condition for a higher Na diffusivity. However, this is not a sufficient condition. Other factors, such as the degree of coupling between anion rotational motion and Na translational motion, as well as the energy landscape of Na migration, also affects the final Na ionic conductivity. In summary, we discovered three novel Na superionic conductors with pronounced cation–anion dynamics coupling: $NaGaBr_4$, $NaNbCl_6$, and Na_4SiSe_4. Their analogues within the same structure group are expected to have low activation energy and high ionic conductivity as well, such as $NaInI_4$, $NaAlI_4$, $NaAlBr_4$, and $NaTaCl_6$.

Exploring the Room-Temperature Ion Dynamics by MLMD. To probe whether the anion dynamics and Na diffusion are still present in our newly discovered superionic conductors at room temperature, we developed machine-

https://doi.org/10.1021/acs.chemmater.4c00102
Chem. Mater. 2024, 36, 3776–3785

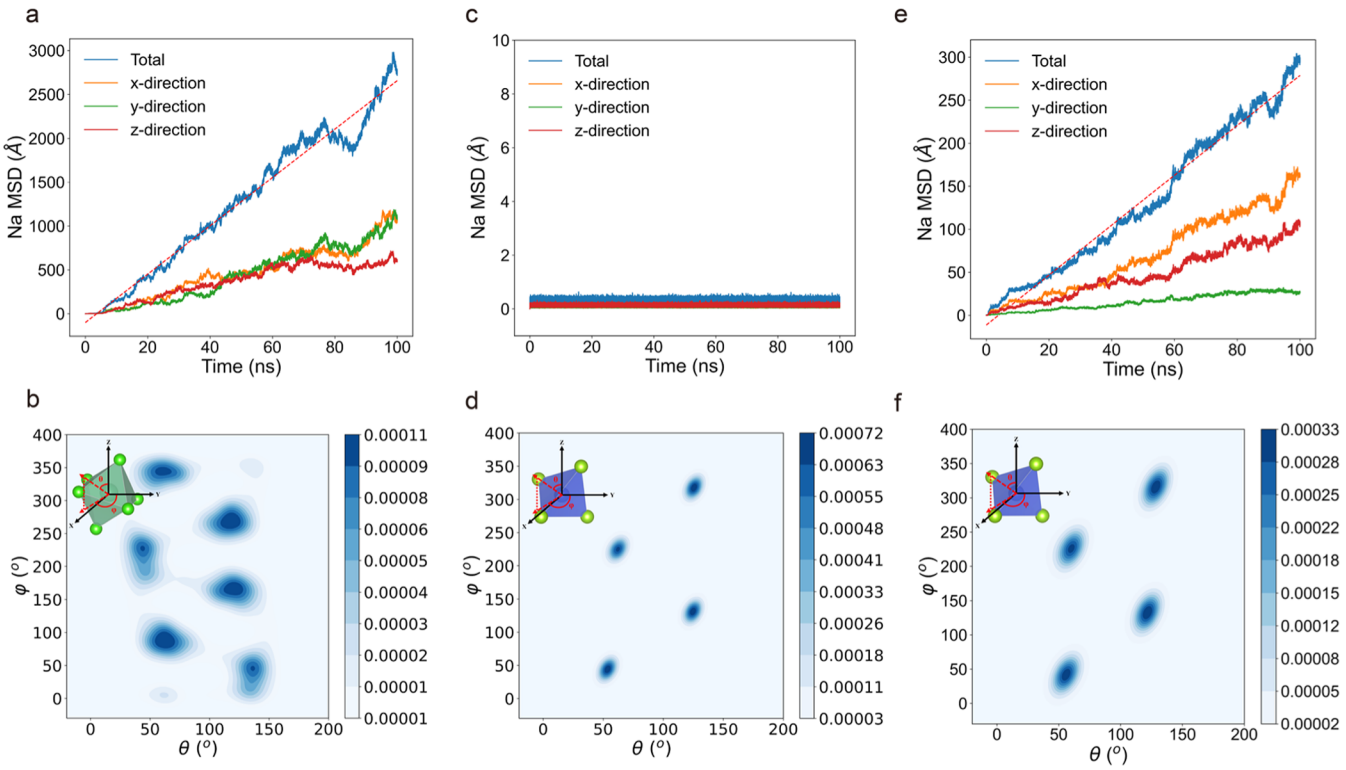

Figure 5. Direction projection Na MSD by 100 ns MLMD simulations at 300 K for (a) $NaNbCl_6$, (c) Na_4SiSe_4, and (e) $Na_{3.75}SiSe_4$. 2D projected probability distribution $\rho(\theta, \varphi)$ of six Cl ligands of Nb16 for $NaNbCl_6$ (b) and four Se ligand of Si34 for Na_4SiSe_4 (d) and $Na_{3.75}SiSe_4$ (f) in a spherical coordinate reference system during the whole MLMD simulations at 300 K, θ is defined as the angle between Nb−Cl or Si−Se bond and z-axis, while angle φ corresponds to angle between the y-axis and the projection of Nb−Cl or Si−Se vector in the xy plane.

learning interatomic potentials based on the moment tensor potential[25] (MTP) formalism for $NaNbCl_6$ and Na_4SiSe_4, and performed long time scale (up to 100 ns) MLMD simulations at 300 K (see Methods for details). Figure 4a,b,d,e shows the mean absolute errors (MAEs) of the fitted MTPs for energies and forces, which are 3.95 meV/atom and 0.10 eV/Å (for $NaNbCl_6$) and 1.34 meV/atom and 0.04 eV/Å (for Na_4SiSe_4), respectively. These MAEs are similar to those of other MTPs fitted in previous work.[22,26] The discrepancy between the training and test MAEs is quite small, suggesting a low probability of overfitting. Additionally, the fitted MTPs for $NaNbCl_6$ and Na_4SiSe_4 reproduce the DFT lattice parameters with an absolute error of less than 2% (Figure 4c,f).

Figure 5a shows the direction projection Na MSD by 100 ns MLMD simulations at 300 K for $NaNbCl_6$, the TMSD is about 3000 $Å^2$, and the x-, y-, and z-direction projected MSD of Na is about 1000 $Å^2$, indicating a significant 3D Na diffusion of $NaNbCl_6$ even at room temperature. The corresponding Na ionic conductivity at 300 K is calculated to be 11.64 mS/cm, which is very close to the $\sigma_{300\,K}$ value (7.67 mS/cm) extrapolated from the AIMD simulations (Figure 3e). The two-dimensional (2D) projected distribution $\rho(\theta, \varphi)$ of the six Cl ligands of $NbCl_6$ octahedra is obtained by mapping the Nb−Cl bond vector in a spherical coordinate reference system, as shown in Figure 5b. During the whole MLMD simulations at 300 K, the six Cl ligands in 16# $NbCl_6$ octahedra exhibit a large-angle distribution around six local maxima, signifying the reorientational/rotational disorder of $NbCl_6$.

For Na_4SiSe_4, the Na ions exhibit only vibration without diffusion at 300 K MLMD simulations (Figure 5c). The 2D projected distribution $\rho(\theta, \varphi)$ of the four Se ligands of $SiSe_4$ tetrahedra only shows four localized spots (Figure 5d), suggesting negligible rotational motion of $SiSe_4$. Viewing the Na MSD and $SiSe_4$ $C(t)$ data obtained through AIMD simulations across temperatures from 900 to 1500 K (see Supporting Information, Figure S22), we found that the diffusion of Na is highly dependent on the rotation of $SiSe_4$. At 900 K, both Na diffusion and the $SiSe_4$ rotation disappear. These results also point to the presence of non-Arrhenius behavior in Na_4SiSe_4, and the room-temperature ionic conductivity of Na_4SiSe_4 extrapolated from the AIMD simulations in the high temperature range is not accurate. Interestingly, in $Na_{3.75}SiSe_4$, we found an enhanced Na diffusion (Figure 5e) and a more intense reorientation of $SiSe_4$ (Figure 5f) by MLMD simulations at 300 K. The calculated room-temperature Na ionic conductivity of $Na_{3.75}SiSe_4$ is up to 4.63 mS/cm. The introduction of Na vacancies is not directly responsible for the enhanced ionic diffusion in $Na_{3.75}SiSe_4$ because if we freeze the Se atoms during a 300 K MLMD simulation in $Na_{3.75}SiSe_4$, Na diffusion becomes negligible (see Supporting Information, Figure S23). Compared to Na_4SiSe_4, $Na_{3.75}SiSe_4$ has a larger free volume due to the reduced Na content, which facilitates the reorientation of Se, thereby leading to enhanced Na diffusion. We suggest that for potential superionic conductors that exhibit the coupled Na-anion dynamics at high temperatures, the introduction of Na vacancies can effectively facilitate both polyanion rotation and Na diffusion, thereby enabling the coupled Na-anion dynamics to be realized at room temperature.

https://doi.org/10.1021/acs.chemmater.4c00102
Chem. Mater. 2024, 36, 3776−3785

CONCLUSIONS

In summary, we design a multistep high-throughput workflow based on the structural feature of isolated framework to search the Na superionic conductors with polyanion rotation. The results of the interpretable machine-learning classification indicate that structures characterized by isolated frameworks, a large volume per atom, and small polyanions are more prone to exhibit anion rotational behavior. For the first time, we observed instance of polyanion rotation behavior in $NaXY_4$ (X = In, Al, Ga; Y = I, Br), $NaXCl_6$ (X = Ta, Nb), Na_4SiSe_4, Na_4TiO_4, Na_3XO_4 (X = V, As), and Na_3NO_4. We conducted a comprehensive analysis of AIMD simulation trajectories to quantify the correlation between anion rotational and Na translational motions for these candidates. As a result, we identified three novel Na superionic conductors that exhibit significant cation−anion dynamics coupling, including $NaXY_4$ (X = In, Al, Ga; Y = I, Br), $NaXCl_6$ (X = Ta, Nb), and Na_4SiSe_4. Their high conductivity is related to the strong coupling of Na vibrational and anion rotational modes in the low-frequency region (<8 THz). Additionally, we developed highly accurate machine-learning interatomic potentials for $NaNbCl_6$ and Na_4SiSe_4. Long time scale (100 ns) MLMD simulations at 300 K revealed that the anion rotation is still present in $NaNbCl_6$ at room temperature, while Na_4SiSe_4 exhibits non-Arrhenius behavior. $Na_{3.75}SiSe_4$ shows an enhanced Na diffusion and a more intense reorientation of $SiSe_4$ at 300 K compared to Na_4SiSe_4. We suggest that for potential superionic conductors that only exhibit the coupled cation−anion dynamics at high temperatures, the introduction of Na vacancies can effectively promote both polyanion rotation and Na diffusion, thus activating the coupled cation−anion dynamics at the low-temperature range. Our work provides guidance for discovery and design of new superionic conductors with polyanion rotation.

METHODS

All calculations was carried out in the framework of density functional theory (DFT)[41] using the projector augmented wave (PAW) method,[42] as implemented in the Vienna Ab initio Simulation Package (VASP). The generalized gradient approximation function parametrized by Perdew−Burke−Ernzerhof (PBE)[43] was employed to describe the exchange−correlation potential. The plane-wave energy cutoff was set to 520 eV, and a k-point density of at least 64/Å^{-3} was employed, similar to that used in the MP database. AIMD simulations for multistep high-throughput workflow were performed without spin-polarization in the canonical (NVT) ensemble at elevated temperatures with a Nosé−Hoover thermostat.[44] A smaller plane-wave energy cutoff of 300 eV was chosen, and a γ-centered 1 × 1 × 1 k-point grid was used to reduce computational expense. Time step was set to 2 fs.

As in a previous literature,[45] the diffusivity D was calculated as the mean square displacement over time interval Δt,

$$D = \frac{1}{2Nd\Delta t}\sum_{i=1}^{N}\langle |r_i(t+\Delta t) - r_i(t)|^2\rangle_t \tag{1}$$

where $d = 3$ is the dimension of the diffusion system, N is the total number of diffusion ions, $r_i(t)$ is the displacement of the ith ion at time t, and the bracket represents averaging over t. The ionic conductivity was calculated according to Nernst−Einstein relationship:

$$\sigma = \frac{nq^2}{k_B T}D \tag{2}$$

where n is the mobile ions volume density, q is the ionic charge, k_B is the Boltzmann constant, and T is the temperature in K.

The diffusivity and temperature satisfy the Arrhenius relationship:

$$D = D_0 \exp\left(-\frac{E_a}{k_B T}\right) \tag{3}$$

which can extrapolate the prefactor D_0, activation energy E_a, diffusivity D, and conductivity σ at room temperature.

The reorientation autocorrelation function $C(t)$ is defined as

$$C(t) = \langle u(t)\cdot u(t=0)\rangle \tag{4}$$

where $u(t)$ is a unit vector from the center atom of polyanion to its anion ligand at time t. < > denotes averaged across all anions of the same species. The rate at which this function decays to zero reflects the reorientation rate of that species.

The functional $h_i(t; a, \Delta t, t_a)$,[46,47] which identifies long-lived Na displacements with a minimum distance a occurring at time t:

$$h_i(t; a, \Delta t, t_a) = \prod_{t'=t_a/2-\Delta t}^{t_a/2} \theta(|r_i(t+t') - r_i(t-t')| - a) \tag{5}$$

where $\theta(x)$ is the Heaviside step function, $\theta(x) = 1$ or 0 for $x \geq 0$ or <0, respectively. $r_i(t)$ represents the displacement of atom i at time t. a is the displacement cutoff used to identify the significant migration of Na (see the caption for exact values). $\Delta t = 3$ ps is the residence time before and after the displacement event and ensures that these displacements are long-lived. $t_a = 9$ ps is a longer time window, including the residence and transition times. $h_i = 1$ represents that the atom i undergoes such a displacement; otherwise, $h_i = 0$.

The moment tensor potential[25] (MTP) for $NaNbCl_6$ and Na_4SiSe_4 was developed using MLIP[48] and the Materials Machine Learning (maml) Python package. To diversify the training structures, 1800 snapshots were uniformly extracted from supercell AIMD simulations in the NPT ensemble at six different temperatures (from 300 to 1300 K with 200 K intervals). Static DFT calculations were performed with a k-point density of at least 100/Å^{-3}, an energy cutoff of 520 eV, and an energy convergence criterion of 10^{-6} eV/atom to obtain accurate energies and forces. For MTPs fitting, a training/test split of 80:20 was used. The radius cutoff R_{cut} that determines the maximum interaction range between atoms was set to 5 Å. The maximum level (lev_{max}) of basis set function were chosen as 8 for $NaNbCl_6$ and 18 for Na_4SiSe_4. Classical MD simulations using the MTP, called machine-learning molecular dynamics (MLMD), were carried out using LAMMPS[49] in the NVT ensemble for 100 ns. The time step was set to 1 fs. The supercells of $NaNbCl_6$ and Na_4SiSe_4 for MLMD simulations are the same as those of AIMD simulations.

ASSOCIATED CONTENT

Data Availability Statement

Data supporting the findings of this study are available from the corresponding author on reasonable request.

Supporting Information

The Supporting Information is available free of charge at https://pubs.acs.org/doi/10.1021/acs.chemmater.4c00102.

Pearson correlation map, F1 score of logistic regression model, uncertainty in diffusion coefficients, species projection MSD, reorientation autocorrelation function, probability density distribution, evolutions of bond length, displacements plots for Na and polyanion, calculated power spectrum, displacement correlation coefficient, AIMD diagnosis information for isolated framework, descriptors for binary classification, cross-validation, and hyperparameter tuning (PDF)

https://doi.org/10.1021/acs.chemmater.4c00102
Chem. Mater. 2024, 36, 3776−3785

AUTHOR INFORMATION

Corresponding Author

Hong Zhu − *University of Michigan-Shanghai Jiao Tong University Joint Institute, Shanghai Jiao Tong University, Shanghai 200240, China;* orcid.org/0000-0001-7919-5661; Email: hong.zhu@sjtu.edu.cn

Authors

Yu Yang − *University of Michigan-Shanghai Jiao Tong University Joint Institute, Shanghai Jiao Tong University, Shanghai 200240, China*

Chaohong Guan − *University of Michigan-Shanghai Jiao Tong University Joint Institute, Shanghai Jiao Tong University, Shanghai 200240, China*

Runxin Ouyang − *University of Michigan-Shanghai Jiao Tong University Joint Institute, Shanghai Jiao Tong University, Shanghai 200240, China*

Complete contact information is available at: https://pubs.acs.org/10.1021/acs.chemmater.4c00102

Author Contributions

Y.Y. and H.Z. designed and guided this research, Y.Y. performed all of the calculations and wrote the paper, and C.G. and R.O. revised the paper and made suggestions. All authors discussed and commented on the paper.

Notes

The authors declare no competing financial interest.

ACKNOWLEDGMENTS

This work was supported by the National Natural Science Foundation of China (52072240) and the Materials Genome Initiative Center at Shanghai Jiao Tong University. All calculations were carried out on the π 2.0 cluster supported by the Center for High Performance Computing at Shanghai Jiao Tong University.

REFERENCES

(1) Kang, B.; Ceder, G. Battery Materials for Ultrafast Charging and Discharging. *Nature* **2009**, *458* (7235), 190−193.

(2) Goodenough, J. B.; Park, K.-S. The Li-Ion Rechargeable Battery: A Perspective. *J. Am. Chem. Soc.* **2013**, *135* (4), 1167−1176.

(3) Janek, J.; Zeier, W. G. A Solid Future for Battery Development. *Nat. Energy* **2016**, *1* (9), No. 16141.

(4) Wu, E. A.; Banerjee, S.; Tang, H.; Richardson, P. M.; Doux, J.-M.; Qi, J.; Zhu, Z.; Grenier, A.; Li, Y.; Zhao, E.; Deysher, G.; Sebti, E.; Nguyen, H.; Stephens, R.; Verbist, G.; Chapman, K. W.; Clément, R. J.; Banerjee, A.; Meng, Y. S.; Ong, S. P. A Stable Cathode-Solid Electrolyte Composite for High-Voltage, Long-Cycle-Life Solid-State Sodium-Ion Batteries. *Nat. Commun.* **2021**, *12* (1), No. 1256.

(5) Famprikis, T.; Bouyanfif, H.; Canepa, P.; Zbiri, M.; Dawson, J. A.; Suard, E.; Fauth, F.; Playford, H. Y.; Dambournet, D.; Borkiewicz, O. J.; Courty, M.; Clemens, O.; Chotard, J.-N.; Islam, M. S.; Masquelier, C. Insights into the Rich Polymorphism of the Na^+ Ion Conductor Na_3PS_4 from the Perspective of Variable-Temperature Diffraction and Spectroscopy. *Chem. Mater.* **2021**, *33* (14), 5652−5667.

(6) Jang, S.-H.; Tateyama, Y.; Jalem, R. High-Throughput Data-Driven Prediction of Stable High-Performance Na-Ion Sulfide Solid Electrolytes. *Adv. Funct. Mater.* **2022**, *32* (48), No. 2206036.

(7) Famprikis, T.; Kudu, Ö. U.; Dawson, J. A.; Canepa, P.; Fauth, F.; Suard, E.; Zbiri, M.; Dambournet, D.; Borkiewicz, O. J.; Bouyanfif, H.; Emge, S. P.; Cretu, S.; Chotard, J.-N.; Grey, C. P.; Zeier, W. G.; Islam, M. S.; Masquelier, C. Under Pressure: Mechanochemical Effects on Structure and Ion Conduction in the Sodium-Ion Solid Electrolyte Na_3PS_4. *J. Am. Chem. Soc.* **2020**, *142* (43), 18422−18436.

(8) Xu, Z.; Chen, X.; Zhu, H.; Li, X. Anharmonic Cation−Anion Coupling Dynamics Assisted Lithium-Ion Diffusion in Sulfide Solid Electrolytes. *Adv. Mater.* **2022**, *34* (49), No. 2207411.

(9) Wang, Y.; Richards, W. D.; Ong, S. P.; Miara, L. J.; Kim, J. C.; Mo, Y.; Ceder, G. Design Principles for Solid-State Lithium Superionic Conductors. *Nat. Mater.* **2015**, *14* (10), 1026−1031.

(10) Jun, K.; Sun, Y.; Xiao, Y.; Zeng, Y.; Kim, R.; Kim, H.; Miara, L. J.; Im, D.; Wang, Y.; Ceder, G. Lithium Superionic Conductors with Corner-Sharing Frameworks. *Nat. Mater.* **2022**, *21* (8), 924−931.

(11) Xiao, Y.; Jun, K.; Wang, Y.; Miara, L. J.; Tu, Q.; Ceder, G. Lithium Oxide Superionic Conductors Inspired by Garnet and NASICON Structures. *Adv. Energy Mater.* **2021**, *11* (37), No. 2101437.

(12) He, X.; Bai, Q.; Liu, Y.; Nolan, A. M.; Ling, C.; Mo, Y. Crystal Structural Framework of Lithium Super-Ionic Conductors. *Adv. Energy Mater.* **2019**, *9* (43), No. 1902078.

(13) Jansen, M. Volume Effect or Paddle-Wheel Mechanism—Fast Alkali-Metal Ionic Conduction in Solids with Rotationally Disordered Complex Anions. *Angew. Chem., Int. Ed.* **1991**, *30* (12), 1547−1558.

(14) Till, P.; Agne, M. T.; Kraft, M. A.; Courty, M.; Famprikis, T.; Ghidiu, M.; Krauskopf, T.; Masquelier, C.; Zeier, W. G. Two-Dimensional Substitution Series $Na_3P_{1-x}Sb_xS_{4-y}Se_y$: Beyond Static Description of Structural Bottlenecks for Na^+ Transport. *Chem. Mater.* **2022**, *34* (5), 2410−2421.

(15) Zhang, Z.; Roy, P.-N.; Li, H.; Avdeev, M.; Nazar, L. F. Coupled Cation−Anion Dynamics Enhances Cation Mobility in Room-Temperature Superionic Solid-State Electrolytes. *J. Am. Chem. Soc.* **2019**, *141* (49), 19360−19372.

(16) Zhang, Z.; Li, H.; Kaup, K.; Zhou, L.; Roy, P.-N.; Nazar, L. F. Targeting Superionic Conductivity by Turning on Anion Rotation at Room Temperature in Fast Ion Conductors. *Matter* **2020**, *2* (6), 1667−1684.

(17) Forrester, F. N.; Quirk, J. A.; Famprikis, T.; Dawson, J. A. Disentangling Cation and Anion Dynamics in Li3PS4 Solid Electrolytes. *Chem. Mater.* **2022**, *34* (23), 10561−10571.

(18) Sun, Y.; Ouyang, B.; Wang, Y.; Zhang, Y.; Sun, S.; Cai, Z.; Lacivita, V.; Guo, Y.; Ceder, G. Enhanced Ionic Conductivity and Lack of Paddle-Wheel Effect in Pseudohalogen-Substituted Li Argyrodites. *Matter* **2022**, *5* (12), 4379−4395.

(19) Fang, H.; Jena, P. Argyrodite-Type Advanced Lithium Conductors and Transport Mechanisms beyond Paddle-Wheel Effect. *Nat. Commun.* **2022**, *13* (1), No. 2078.

(20) Guan, C.; Yang, Y.; Ouyang, R.; Jing, H.; Yan, J.; Zhu, H. Enhanced Ionic Conductivity of Protonated Antiperovskites *via* Tuning Lattice and Rotational Dynamics. *J. Mater. Chem. A* **2023**, *11* (12), 6157−6167.

(21) Tsai, P.-C.; Mair, S.; Smith, J.; Halat, D. M.; Chien, P.-H.; Kim, K.; Zhang, D.; Li, Y.; Yin, L.; Liu, J.; Lapidus, S. H.; Reimer, J. A.; Balsara, N. P.; Siegel, D. J.; Chiang, Y.-M. Double Paddle-Wheel Enhanced Sodium Ion Conduction in an Antiperovskite Solid Electrolyte. *Adv. Energy Mater.* **2023**, *13* (7), No. 2203284.

(22) Xu, Z.; Duan, H.; Dou, Z.; Zheng, M.; Lin, Y.; Xia, Y.; Zhao, H.; Xia, Y. Machine Learning Molecular Dynamics Simulation Identifying Weakly Negative Effect of Polyanion Rotation on Li-Ion Migration. *npj Comput. Mater.* **2023**, *9* (1), No. 2000077.

(23) Effat, M. B.; Liu, J.; Lu, Z.; Wan, T. H.; Curcio, A.; Ciucci, F. Stability, Elastic Properties, and the Li Transport Mechanism of the Protonated and Fluorinated Antiperovskite Lithium Conductors. *ACS Appl. Mater. Interfaces* **2020**, *12* (49), 55011−55022.

(24) Krenzer, G.; Klarbring, J.; Tolborg, K.; Rossignol, H.; McCluskey, A. R.; Morgan, B. J.; Walsh, A. Nature of the Superionic Phase Transition of Lithium Nitride from Machine Learning Force Fields. *Chem. Mater.* **2023**, *35* (15), 6133−6140.

(25) Shapeev, A. V. Moment Tensor Potentials: A Class of Systematically Improvable Interatomic Potentials. *Multiscale Model. Simul.* **2016**, *14* (3), 1153−1173.

(26) Qi, J.; Banerjee, S.; Zuo, Y.; Chen, C.; Zhu, Z.; Holekevi Chandrappa, M. L.; Li, X.; Ong, S. P. Bridging the Gap between

Simulated and Experimental Ionic Conductivities in Lithium Superionic Conductors. *Mater. Today Phys.* **2021**, *21*, No. 100463.
(27) Jain, A.; Ong, S. P.; Hautier, G.; Chen, W.; Richards, W. D.; Dacek, S.; Cholia, S.; Gunter, D.; Skinner, D.; Ceder, G.; Persson, K. A. Commentary: The Materials Project: A Materials Genome Approach to Accelerating Materials Innovation. *APL Mater.* **2013**, *1* (1), No. 011002.
(28) Deng, Z.; Zhu, Z.; Chu, I.-H.; Ong, S. P. Data-Driven First-Principles Methods for the Study and Design of Alkali Superionic Conductors. *Chem. Mater.* **2017**, *29* (1), 281−288.
(29) Wang, S.; Bai, Q.; Nolan, A. M.; Liu, Y.; Gong, S.; Sun, Q.; Mo, Y. Lithium Chlorides and Bromides as Promising Solid-State Chemistries for Fast Ion Conductors with Good Electrochemical Stability. *Angew. Chem., Int. Ed.* **2019**, *58* (24), 8039−8043.
(30) He, X.; Zhu, Y.; Mo, Y. Origin of Fast Ion Diffusion in Super-Ionic Conductors. *Nat. Commun.* **2017**, *8* (1), No. 15893.
(31) Wang, Y.; Richards, W. D.; Bo, S.-H.; Miara, L. J.; Ceder, G. Computational Prediction and Evaluation of Solid-State Sodium Superionic Conductors $Na_7P_3X_{11}$ (X = O, S, Se). *Chem. Mater.* **2017**, *29* (17), 7475−7482.
(32) Smith, J. G.; Siegel, D. J. Ion Migration Mechanisms in the Sodium Sulfide Solid Electrolyte $Na_{3-x}Sb_{1-x}W_xS_4$. *Chem. Mater.* **2022**, *34* (9), 4166−4171.
(33) Sendek, A. D.; Yang, Q.; Cubuk, E. D.; Duerloo, N. K.-A.; Cui, Y.; Reed, J. E. Holistic Computational Structure Screening of More than 12000 Candidates for Solid Lithium-Ion Conductor Materials. *Energy Environ. Sci.* **2017**, *10* (1), 306−320.
(34) Kim, K.; Siegel, D. J. Machine Learning Reveals Factors That Control Ion Mobility in Anti-Perovskite Solid Electrolytes. *J. Mater. Chem. A* **2022**, *10* (28), 15169−15182.
(35) Pedregosa, F.; Varoquaux, G.; Gramfort, A.; Michel, V.; Thirion, B.; Grisel, O.; Blondel, M.; Prettenhofer, P.; Weiss, R.; Dubourg, V.; Vanderplas, J.; Passos, A.; Cournapeau, D.; Brucher, M.; Perrot, M.; Duchesnay, É. Scikit-learn: Machine Learning in Python. *J. Mach. Learn. Res.* **2011**, *12*, 2825−2830.
(36) Lundberg, S. M.; Lee, S.-I. A Unified Approach to Interpreting Model Predictions. In *Proceedings of the 31st International Conference on Neural Information Processing Systems*; von Luxburg, U., Ed.; NIPS, 2017; pp 4768−4777.
(37) Ong, S. P.; Richards, W. D.; Jain, A.; Hautier, G.; Kocher, M.; Cholia, S.; Gunter, D.; Chevrier, V. L.; Persson, K. A.; Ceder, G. Python Materials Genomics (Pymatgen): A Robust, Open-Source Python Library for Materials Analysis. *Comput. Mater. Sci.* **2013**, *68*, 314−319.
(38) Wilmer, D.; Banhatti, R. D.; Fitter, J.; Funke, K.; Jansen, M.; Korus, G.; Lechner, R. E. Anion Reorientation in Na_3PO_4. *Phys. B* **1997**, *241*−*243*, 338−340.
(39) Yang, Y.; Xu, Z.; Guan, C.; Ouyang, R.; Jing, H.; Zhu, H. Activating the Paddle-Wheel Effect towards Lower Temperature in a New Sodium-Ion Solid Electrolyte, $Na_{3.5}Si_{0.5}P_{0.5}Se_4$. *J. Mater. Chem. A* **2023**, *11* (17), 9555−9565.
(40) Muy, S.; C Bachman, J.; Giordano, L.; Chang, H.-H.; L Abernathy, D.; Bansal, D.; Delaire, O.; Hori, S.; Kanno, R.; Maglia, F.; Lupart, S.; Lamp, P.; Shao-Horn, Y. Tuning Mobility and Stability of Lithium Ion Conductors Based on Lattice Dynamics. *Energy Environ. Sci.* **2018**, *11* (4), 850−859.
(41) Kohn, W.; Sham, L. J. Self-Consistent Equations Including Exchange and Correlation Effects. *Phys. Rev.* **1965**, *140* (4), A1133−A1138.
(42) Blöchl, P. E. Projector Augmented-Wave Method. *Phys. Rev. B* **1994**, *50* (24), 17953−17979.
(43) Perdew, J. P.; Burke, K.; Ernzerhof, M. Generalized Gradient Approximation Made Simple. *Phys. Rev. Lett.* **1996**, *77* (18), 3865−3868.
(44) Hoover, W. G. Canonical Dynamics: Equilibrium Phase-Space Distributions. *Phys. Rev. A* **1985**, *31* (3), 1695−1697.
(45) He, X.; Zhu, Y.; Epstein, A.; Mo, Y. Statistical Variances of Diffusional Properties from Ab Initio Molecular Dynamics Simulations. *npj Comput. Mater.* **2018**, *4* (1), 18.
(46) Burbano, M.; Carlier, D.; Boucher, F.; Morgan, B. J.; Salanne, M. Sparse Cyclic Excitations Explain the Low Ionic Conductivity of Stoichiometric $Li_7La_3Zr_2O_{12}$. *Phys. Rev. Lett.* **2016**, *116* (13), No. 135901.
(47) Smith, J. G.; Siegel, D. J. Low-Temperature Paddlewheel Effect in Glassy Solid Electrolytes. *Nat. Commun.* **2020**, *11* (1), No. 1483.
(48) Novikov, I. S.; Gubaev, K.; Podryabinkin, E. V.; Shapeev, A. V. The MLIP Package: Moment Tensor Potentials with MPI and Active Learning. *Mach. Learn.: Sci. Technol.* **2021**, *2* (2), No. 025002.
(49) Plimpton, S. Fast Parallel Algorithms for Short-Range Molecular Dynamics. *J. Comput. Phys.* **1995**, *117* (1), 1−19.

https://doi.org/10.1021/acs.chemmater.4c00102
Chem. Mater. 2024, 36, 3776−3785